

Floquet Quadrupole Photonic Crystals Protected by Space-Time Symmetry

Jicheng Jin¹, Li He, Jian Lu¹, Eugene J. Mele¹, and Bo Zhen^{1*}

Department of Physics and Astronomy, University of Pennsylvania, Philadelphia, Pennsylvania 19104, USA

 (Received 12 May 2021; revised 25 August 2021; accepted 19 July 2022; published 4 August 2022)

High-order topological phases, such as those with nontrivial quadrupole moments [1,2], protect edge states that are themselves topological insulators in lower dimensions. So far, most quadrupole phases of light are explored in linear optical systems, which are protected by spatial symmetries [3] or synthetic symmetries [1,2,4–7]. Here we present Floquet quadrupole phases in driven nonlinear photonic crystals that are protected by space-time screw symmetries [8]. We start by illustrating space-time symmetries by tracking the trajectory of instantaneous optical axes of the driven media. Our Floquet quadrupole phase is then confirmed in two independent ways: symmetry indices at high-symmetry momentum points and calculations of the nested Wannier bands. Our Letter presents a general framework to analyze symmetries in driven optical materials and paves the way to further exploring symmetry-protected topological phases in Floquet systems and their optoelectronic applications.

DOI: 10.1103/PhysRevLett.129.063902

Symmetry plays an important role in topological phases [9–14]. Examples include topological insulators that are protected by time-reversal symmetry [15,16], Chern insulators that require breaking time-reversal symmetry [17–20], and topological crystalline insulators [21] that are protected by spatial symmetries such as rotation and reflection. One important class of topological crystalline insulators is high-order topological insulators [1,6,7,22–27], where the interesting physical consequences appear in spaces two or more dimensions lower than the bulk. For example, quadrupole topological insulators in two dimensions, characterized by their quantized and nontrivial second-order moments, protect zero-dimensional corner states with fractional occupations. So far, most studied quadrupole phases of light are protected by synthetic symmetries in the lattice model—such as the notion of π fluxes [1,5,7]—or spatial symmetries such as the fourfold rotation [3]. Moving beyond linear optics, a different class of Floquet topological phases can be found in nonlinear materials driven by time-varying fields. While some examples of Floquet topological phases have been explored [4,28–30], detailed symmetry analysis, in both space and time, and the general recipe to achieve symmetry-protected topological phases in driven nonlinear optical systems remain largely unexplored.

Here we present Floquet quadrupole phases in driven nonlinear PhCs, where the quadrupole moments are quantized and protected by a space-time screw symmetry, involving both rotation in space and translation in time. This differs from previous studies, which are based on purely spatial symmetry [3,31] or the tight-binding approximation. While space-time screw symmetry also

exists in other systems (e.g., circularly shaken cold atom lattices [32–34] and light irradiated graphene [35–37]), previous studies mostly focus on Chern insulators, which do not rely on the space-time symmetries, leaving them largely unexplored. Differently, our Floquet quadrupole phase here is protected by space-time symmetry. We define and analyze this space-time symmetry in a specific example of driven GaAs before presenting the detailed design of a Floquet quadrupole PhC. The nontrivial quadrupole moment is then confirmed with the numerical calculations of the nested Wilson loops. Finally, we demonstrate key features associated with quadrupole phases, including fractional corner occupations and filling anomalies [3,22].

We first define the space-time screw symmetry in a driven nonlinear medium. As shown in Fig. 1(a), a circularly polarized field $\mathbf{E}_d = E_d \cos(\Omega t)\hat{x} + E_d \sin(\Omega t)\hat{y}$ periodically drives a uniform slab of GaAs. This driving field couples to the second-order nonlinear susceptibility of

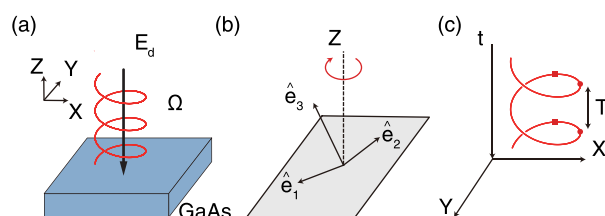


FIG. 1. Space-time screw symmetry in a driven nonlinear medium. (a) Schematic of a uniform slab of GaAs driven by a circularly polarized field \mathbf{E}_d incident from the normal direction. (b) All three instantaneous optical axes of the driven medium, \hat{e}_{1-3} , spin around the z axis. (c) Screw symmetry can be found in each of the optical axes, defined through a combination of rotation in space (x, y) and translation in time (t).

GaAs, $\chi_{xyz}^{(2)}$ and its permutations, and gives rise to a time-dependent permittivity:

$$\bar{\epsilon}(t) = \begin{pmatrix} \epsilon & 0 & \alpha \sin(\Omega t) \\ 0 & \epsilon & \alpha \cos(\Omega t) \\ \alpha \sin(\Omega t) & \alpha \cos(\Omega t) & \epsilon \end{pmatrix}. \quad (1)$$

Here, ϵ is the linear permittivity of GaAs that is isotropic and $\alpha = 2\chi_{xyz}^{(2)}E_d$ is the nonlinear perturbation. Higher-order perturbations are ignored here under the assumption of a weak driving field. To determine the symmetry of this driven medium, we analyze the temporal evolution of its three optical axes:

$$\begin{aligned} \hat{e}_1 &= \cos(\Omega t)\hat{x} - \sin(\Omega t)\hat{y}, \\ \hat{e}_2 &= \frac{1}{\sqrt{2}}[\sin(\Omega t)\hat{x} + \cos(\Omega t)\hat{y} - \hat{z}], \\ \hat{e}_3 &= \frac{1}{\sqrt{2}}[\sin(\Omega t)\hat{x} + \cos(\Omega t)\hat{y} + \hat{z}]. \end{aligned} \quad (2)$$

As shown in Fig. 1(b), all three optical axes spin around the z axis at the driving frequency Ω . We can further trace out the trajectory of the optical axes in both space (x, y) and time (t). An example for \hat{e}_1 is shown in Fig. 1(c), which evolves along a helix. This provides the foundation for our symmetry analysis below.

First, we note that the driving field breaks the continuous rotation symmetry of the isotropic linear permittivity of GaAs; namely, the helix in Fig. 1(c) does not return to itself if it is rotated by some general angle in the xy plane (e.g., 90°). Instead, it has a symmetry involving a compound operation with a rotation in space and a shift in time. For example, one can first rotate the helix by 90° along the counterclockwise direction in the xy plane (C_4) and then translate it by $T/4$ in time ($\hat{T}_{T/4}$). Here $T = 2\pi/\Omega$ is the periodicity of the driving field. For convenience, we denote this space-time screw operation as

$$\tilde{S}_4 = \hat{O}_{C_4} \times \hat{T}_{T/4}. \quad (3)$$

Naturally, if one repeats this \tilde{S}_4 operation four times, the whole system evolves in time by a full periodicity T and, thus, remains unchanged. Under this requirement of $(\tilde{S}_4)^4 = 1$, the four allowed \tilde{S}_4 symmetry indices are ± 1 and $\pm i$. The symmetry of this driven medium can also be derived by checking the commutation rules between various symmetry operations and the time-dependent nonlinear permittivity, reaching the same conclusions. See Sec. I of the Supplemental Material [38] for more details.

We stress that, as the symmetry analysis is on the effective permittivity, it is not uniquely defined by the driving field; instead, it also depends on the exact form of optical nonlinearity provided by the material. For example,

an x -cut LiNbO₃ driven by a z -polarized field will have not a space-time symmetry but a purely spatial symmetry of C_2^x [31].

Next, we present a concrete example of Floquet quadrupole photonic crystal (PhC) that is protected by this space-time symmetry of \tilde{S}_4 . The 2D PhC consists of veins and disks made from GaAs in the air, and one unit cell with periodic boundaries is presented in Fig. 2(a). Veins of width $w = 50$ nm form a square lattice of periodicity $a = 500$ nm. Four disks of diameter $d = 348$ nm are arranged in a C_4 symmetric way in each unit cell. The calculated PhC band structure, eigenfrequencies ω as functions of momentum k , is shown in Fig. 2(b), where TE modes (E_x, E_y, H_z) and TM modes (H_x, H_y, E_z) are colored in blue and red, respectively. By engineering the location and size of the disks, four of the bands are well isolated from the rest, each residing inside a TE or TM band gap that is shaded in blue or red.

A circularly polarized driving field E_d is applied on the PhC and the topology is further explored by studying the Floquet eigenstates. These Floquet eigenstates can be probed by a weak probe beam in a potential experimental demonstration using a pump-probe setup. The pump field E_d is nondepletable, which solely defines the time-dependent permittivity. Thus, similar to our previous analysis, the spatial rotation symmetry C_4 is broken in this PhC. Instead, the PhC now has a space-time screw symmetry \tilde{S}_4 , which quantizes bulk dipole and quadrupole moments. See Sec. II in the Supplemental Material [38] for detailed derivations. The bulk quadrupole moment q_{xy} of two isolated bands can be evaluated using the \tilde{S}_4 symmetry indices at their high-symmetry momentum points as

$$e^{i2\pi q_{xy}} = \tilde{S}_4^+(\Gamma)\tilde{S}_4^{+*}(M) = \tilde{S}_4^-(\Gamma)\tilde{S}_4^{-*}(M). \quad (4)$$

Since four applications of \tilde{S}_4 restore the system, we have $(\tilde{S}_4)^4 = 1$ and $(\tilde{S}_4)^2 = \pm 1$. Here in Eq. (4), \tilde{S}_4^\pm refers to the \tilde{S}_4 eigenvalue of a mode with an $(\tilde{S}_4)^2$ eigenvalue of ± 1 . Naturally, $\tilde{S}_4^+ = \pm 1$ and $\tilde{S}_4^- = \pm i$. Based on these symmetry indices at high-symmetry momentum points, we observe that $e^{i2\pi q_{xy}} = \pm 1$ give rise to trivial (nontrivial) quadrupole moment $q_{xy} = 0(1/2)$. Based on this formalism, we later show how to achieve nontrivial quadrupole moments through driving fields.

To find the Floquet eigenstates of this driven PhC and their relevant \tilde{S}_4 indices, we solve the Floquet eigenvalue problem of Maxwell's equations, following our previous theoretical framework [29]. We note that since the Floquet eigenstates are free to exchange energy with the nondepletable pump by emitting or absorbing a pump photon the Floquet eigenvalue problem is generically non-Hermitian [39]. In short, we expand the Floquet eigenstates using the Floquet basis as $\Phi(t) = e^{-i\lambda t} \sum_{jm} c_{jm} |j, m\rangle$ and then compute the Floquet eigenvalues λ and coefficients

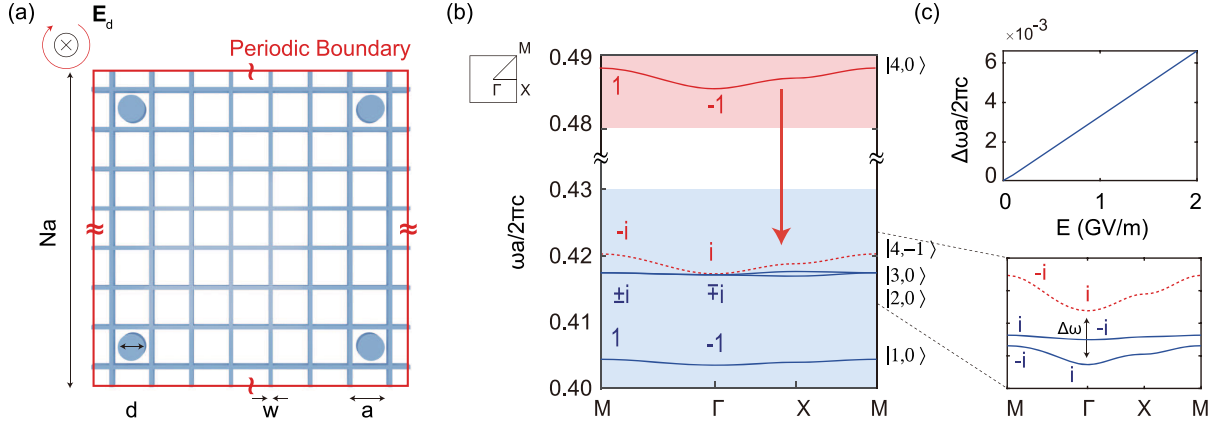


FIG. 2. Space-time symmetry indices of photonic bands dressed by optical nonlinearity. (a) Schematic drawing of a square GaAs PhC unit cell with periodicity Na ($N = 8$), consisting of veins of width w and spacing a as well as 4 disks of diameter d . (b) The PhC band structure, including both TE (blue lines) and TM bands (red). The \tilde{S}_4 symmetry indices are labeled at the high-symmetry momentum points (Γ and M) of each band. If driven by an external field, Floquet basis sharing the same \tilde{S}_4 index, such as $|4, -1\rangle$ and $|2, 0\rangle$ at Γ , will couple to each other, which leads to an energy splitting of $\Delta\omega$ and opens a new gap in the Floquet spectrum. (c) The energy splitting $\Delta\omega$ increases linearly with the driving field strength E .

c_{jm} . Floquet basis states $|j, m\rangle = |j\rangle e^{im\Omega t}$ are essentially copies of the static PhC eigenstate $|j\rangle$, but shifted in frequency by $m\Omega$. One example is the Floquet basis $|4, -1\rangle$ shown in Fig. 2(b), which is shifted down by Ω from $|4, 0\rangle$.

To understand the \tilde{S}_4 indices of the Floquet eigenstates, we start by comparing the symmetries under C_4 and the compound operation \tilde{S}_4 .

$$\hat{O}_{\tilde{S}_4}|j, m\rangle = (\zeta_j \times i^m)|j, m\rangle, \quad (5)$$

$$\hat{O}_{\tilde{S}_4}|j, 0\rangle = \zeta_j|j, 0\rangle. \quad (6)$$

Here $\hat{O}_{\tilde{S}_4}$ refers to the space-time screw operation on a time-dependent vector field. One example of the $\hat{O}_{\tilde{S}_4}$ operation is shown in Sec. II in the Supplemental Material [38]. Namely, the \tilde{S}_4 index depends on the band information j and the Floquet order m . For example, for $m = 0$, the \tilde{S}_4 index reduces to C_4 index ζ_j of $|j\rangle$; for $m = \pm 1$, the \tilde{S}_4 index is changed by $\pm i$. This dressing process can also be understood intuitively without the Floquet basis by checking the spatial symmetry indices of the nonlinear dipoles of sum or difference frequency generation. Our detailed derivations can be found in Sec. III of the Supplemental Material [38]. Naturally, the \tilde{S}_4 index of a Floquet eigenstate is the same as that of all of its constituting Floquet basis.

We now apply this symmetry analysis to our specific setup and compute the quadrupole moment. When the Floquet basis $|4, 0\rangle$ shifts down in frequency to $|4, -1\rangle$, its \tilde{S}_4 index at Γ changes from -1 to $+i$, which is now the same as the \tilde{S}_4 index of $|2, 0\rangle$. Naturally, the two Floquet basis, $|4, -1\rangle$ and $|2, 0\rangle$, will couple to each other under a

driving field, resulting in an energy splitting $\Delta\omega$ between them. This energy splitting increases linearly with the driving field strength [Fig. 2(c)], lifts the degeneracy between static states $|2, 0\rangle$ and $|3, 0\rangle$, and opens a new (Floquet) energy gap. Using Eq. (4), the quadrupole moment of the two bands below the Floquet gap, $|1, 0\rangle$ and $|2, 0\rangle$, can be evaluated as $e^{i2\pi q_{xy}} = -1$ and $q_{xy} = 1/2$; namely, we have now achieved a Floquet quadrupole phase.

Next, we confirm the Floquet quadrupole phase through direct calculations of the nested Wannier bands. To this end, we first compute the Wannier bands $\nu_{x,y}$ of the two Floquet bands of interest, $|1, 0\rangle$ and $|2, 0\rangle$, which are the phases of the eigenvalues of the Wilson loop $W_{x(y), \mathbf{k}_j + 2\pi\hat{\mathbf{x}}(\hat{\mathbf{y}}) \leftarrow \mathbf{k}}$. The Wilson loop is defined based on the inner product of adjacent Floquet states in a period-averaged way. We note that due to the non-Hermitian form of our formula, the inner product is defined with left and right eigenvectors. Our results, shown in the upper panel of Fig. 3(a), confirm that we have vanishing dipole moments in both directions: $p_x = p_y = 0$. Besides an energy gap [Fig. 2(c)], the driving field also opens a Wannier gap between the two Wannier bands [Fig. 3(b)], which are gapless without a driving field. This Wannier gap allows one to separate the Wannier bands into two sectors, ν^\pm , and obtain the nested Wannier bands $p_{x(y)}^{\nu^\pm}$ by computing the nested Wilson loop. The nested Wilson loop is defined with Wannier band basis, which are eigenvectors of the Wilson loops. Our results, shown in the lower panel of Fig. 3(a), confirm that our driven PhC indeed has a nontrivial quadrupole moment of $q_{xy} = 2p_x^{\nu_y} p_y^{\nu_x} = 1/2$. Details of the calculation are presented in Sec. IV of the Supplemental Material [38].

Finally, we present the physical consequences of Floquet quadrupole PhCs in the contexts of corner states and filling

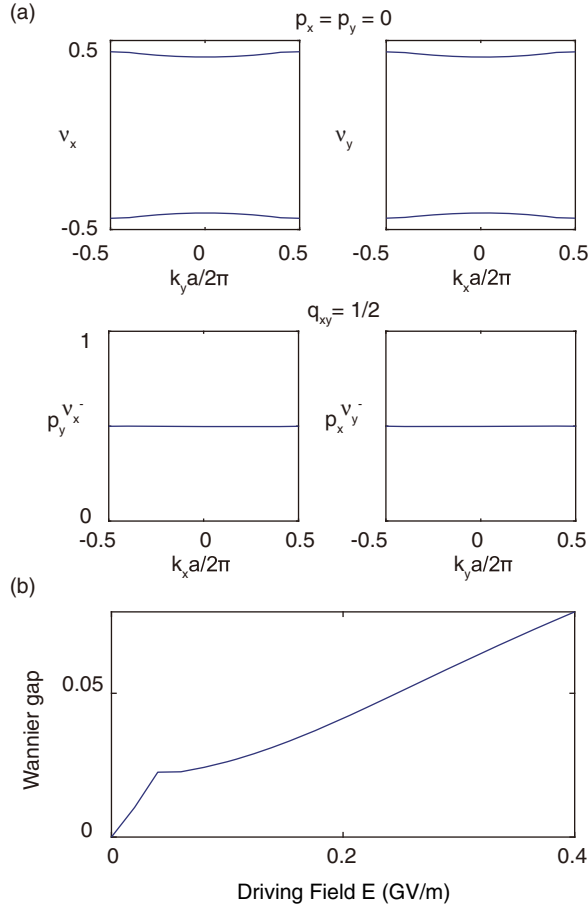


FIG. 3. Confirmation of quadrupole phases through Wannier band calculations. (a) Calculated Wannier bands and nested Wannier bands for the first two Floquet bands. The results confirm the vanishing dipole moments $p_x = p_y = 0$ and the nontrivial quadrupole moment $q_{xy} = 1/2$. (b) The gap between the two Wannier bands is opened by the external driving field.

anomalies. We start by computing the eigenstates in a $N \times N$ supercell of Floquet quadrupole PhCs surrounded by perfect electric conductors (PECs). Our specific setup with $N = 10$ is shown in Fig. 4(a). There is a thin gap between the supercell and the PECs. The eigenstates are labeled in the order of their Floquet eigenvalues. Similar to other quadrupole phases [3,5], we also observe 4 degenerate states in the energy gap [states 199–202 in Fig. 4(b)], which are localized at the four supercell corners. Because of the lack of chiral symmetry expanded around a nonzero frequency in Maxwell’s equations, these corner states are not pinned to the center of the energy gap; instead, they can shift up or down in frequency or even merge into the bulk continuum. A filling anomaly is also confirmed in our system by noting the incompatibility between the number of eigenstates below the Floquet gap ($2N^2 - 2 = 198$) and the number of unit cells in the supercell ($N^2 = 100$). Our quadrupole phase is further confirmed by the fractional

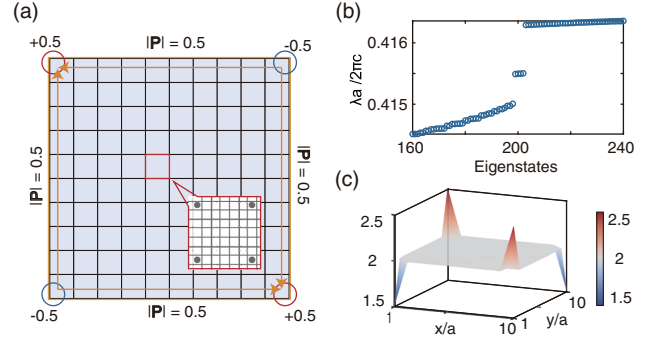


FIG. 4. Physical consequences of corner states and filling anomaly. (a) Schematic of a 10×10 supercell of Floquet quadrupole PhCs. One unit cell is presented in the inset. (b) The eigenvalue spectrum confirms the existence of corner states and the filling anomaly in our system. (c) Accumulative time-averaged energy density profile of the first 200 eigenstates, showing fractional occupations (2 ± 0.5) at the four corners.

occupations at the corners, which is an integral of the mode density over the occupied bands, as shown in Fig. 4(c). In these calculations, the disk diameter d is tuned to place the corner-state frequency in the middle of the Floquet gap. Details of the calculation are presented in Sec. V of the Supplemental Material [38].

In summary, we present Floquet quadrupole phases that are protected by the space-time screw symmetry in a driven nonlinear PhC. The parameters used in our calculations are practical, and the proposed system can be readily studied in nonlinear optical experiments. Furthermore, while our example focuses on GaAs, the space-time symmetry analysis applies to the vast range of nonlinear materials, opening the door to further explorations into new topological phases and consequences in driven systems, such as symmetry-protected topological classification [40] and topological quantum chemistry [41]. Finally, our general formalism of understanding Floquet topological phases in driven systems can extend beyond photonics into other nonlinear wave systems, including phononics, piezoelectrics, piezomagnetism, and polaritonics.

This work was partly supported by the National Science Foundation through the University of Pennsylvania Materials Research Science and Engineering Center DMR-1720530, the U.S. Office of Naval Research (ONR) Multidisciplinary University Research Initiative (MURI) Grant N00014-20-1-2325 on Robust Photonic Materials with High-Order Topological Protection, and the Air Force Office of Scientific Research under Award No. FA9550-18-1-0133. J.L. was also supported by the Army Research Office under Contract No. W911NF-19-1-0087. Work by E.M. was supported by the Department of Energy, Office of Basic Energy Sciences under Grant No. DE FG02 84ER45118.

- *bozhen@sas.upenn.edu
- [1] W. A. Benalcazar, B. A. Bernevig, and T. L. Hughes, Electric multipole moments, topological multipole moment pumping, and chiral hinge states in crystalline insulators, *Phys. Rev. B* **96**, 245115 (2017).
 - [2] W. A. Benalcazar, B. A. Bernevig, and T. L. Hughes, Quantized electric multipole insulators, *Science* **357**, 61 (2017).
 - [3] L. He, Z. Addison, E. J. Mele, and B. Zhen, Quadrupole topological photonic crystals, *Nat. Commun.* **11**, 3119 (2020).
 - [4] A. Dutt, M. Minkov, I. A. D. Williamson, and S. Fan, Higher-order topological insulators in synthetic dimensions, *Light* **9**, 131 (2020).
 - [5] S. Mittal, V. V. Orre, G. Zhu, M. A. Gorlach, A. Poddubny, and M. Hafezi, Photonic quadrupole topological phases, *Nat. Photonics* **13**, 692 (2019).
 - [6] C. W. Peterson, T. Li, W. A. Benalcazar, T. L. Hughes, and G. Bahl, A fractional corner anomaly reveals higher-order topology, *Science* **368**, 1114 (2020).
 - [7] C. W. Peterson, W. A. Benalcazar, T. L. Hughes, and G. Bahl, A quantized microwave quadrupole insulator with topologically protected corner states, *Nature (London)* **555**, 346 (2018).
 - [8] S. Xu and C. Wu, Space-Time Crystal and Space-Time Group, *Phys. Rev. Lett.* **120**, 096401 (2018).
 - [9] C.-K. Chiu, J. C. Y. Teo, A. P. Schnyder, and S. Ryu, Classification of topological quantum matter with symmetries, *Rev. Mod. Phys.* **88**, 035005 (2016).
 - [10] A. P. Schnyder, S. Ryu, A. Furusaki, and A. W. W. Ludwig, Classification of topological insulators and superconductors in three spatial dimensions, *Phys. Rev. B* **78**, 195125 (2008).
 - [11] A. Kitaev, Periodic table for topological insulators and superconductors, *AIP Conf. Proc.* **1134**, 22 (2009).
 - [12] S. Ryu, A. P. Schnyder, A. Furusaki, and A. W. W. Ludwig, Topological insulators and superconductors: Tenfold way and dimensional hierarchy, *New J. Phys.* **12**, 065010 (2010).
 - [13] L. Lu, J. D. Joannopoulos, and M. Soljačić, Topological photonics, *Nat. Photonics* **8**, 821 (2014).
 - [14] T. Ozawa, H. M. Price, A. Amo, N. Goldman, M. Hafezi, L. Lu, M. C. Rechtsman, D. Schuster, J. Simon, O. Zilberberg, and I. Carusotto, Topological photonics, *Rev. Mod. Phys.* **91**, 015006 (2019).
 - [15] C. L. Kane and E. J. Mele, Quantum Spin Hall Effect in Graphene, *Phys. Rev. Lett.* **95**, 226801 (2005).
 - [16] L. Fu and C. L. Kane, Topological insulators with inversion symmetry, *Phys. Rev. B* **76**, 045302 (2007).
 - [17] F. D. M. Haldane and S. Raghu, Possible Realization of Directional Optical Waveguides in Photonic Crystals with Broken Time-Reversal Symmetry, *Phys. Rev. Lett.* **100**, 013904 (2008).
 - [18] Z. Wang, Y. D. Chong, J. D. Joannopoulos, and M. Soljačić, Reflection-Free One-Way Edge Modes in a Gyromagnetic Photonic Crystal, *Phys. Rev. Lett.* **100**, 013905 (2008).
 - [19] Z. Wang, Y. Chong, J. D. Joannopoulos, and M. Soljačić, Observation of unidirectional backscattering-immune topological electromagnetic states, *Nature (London)* **461**, 772 (2009).
 - [20] S. A. Skirlo, L. Lu, Y. Igarashi, Q. Yan, J. Joannopoulos, and M. Soljačić, Experimental Observation of Large Chern Numbers in Photonic Crystals, *Phys. Rev. Lett.* **115**, 253901 (2015).
 - [21] L. Fu, Topological Crystalline Insulators, *Phys. Rev. Lett.* **106**, 106802 (2011).
 - [22] W. A. Benalcazar, T. Li, and T. L. Hughes, Quantization of fractional corner charge in C_n -symmetric higher-order topological crystalline insulators, *Phys. Rev. B* **99**, 245151 (2019).
 - [23] Y. Liu, S. Leung, F.-F. Li, Z.-K. Lin, X. Tao, Y. Poo, and J.-H. Jiang, Bulk-disclination correspondence in topological crystalline insulators, *Nature (London)* **589**, 381 (2021).
 - [24] X. Zhang, H.-X. Wang, Z.-K. Lin, Y. Tian, B. Xie, M.-H. Lu, Y.-F. Chen, and J.-H. Jiang, Second-order topology and multidimensional topological transitions in sonic crystals, *Nat. Phys.* **15**, 582 (2019).
 - [25] X. Zhang, Z.-K. Lin, H.-X. Wang, Z. Xiong, Y. Tian, M.-H. Lu, Y.-F. Chen, and J.-H. Jiang, Symmetry-protected hierarchy of anomalous multipole topological band gaps in nonsymmorphic metacrystals, *Nat. Commun.* **11**, 65 (2020).
 - [26] S. Imhof, C. Berger, F. Bayer, J. Brehm, L. W. Molenkamp, T. Kiessling, F. Schindler, C. H. Lee, M. Greiter, T. Neupert, and R. Thomale, Topoelectrical-circuit realization of topological corner modes, *Nat. Phys.* **14**, 925 (2018).
 - [27] M. Serra-Garcia, V. Peri, R. Süsstrunk, O. R. Bilal, T. Larsen, L. G. Villanueva, and S. D. Huber, Observation of a phononic quadrupole topological insulator, *Nature (London)* **555**, 342 (2018).
 - [28] M. C. Rechtsman, J. M. Zeuner, Y. Plotnik, Y. Lumer, D. Podolsky, F. Dreisow, S. Nolte, M. Segev, and A. Szameit, Photonic floquet topological insulators, *Nature (London)* **496**, 196 (2013).
 - [29] L. He, Z. Addison, J. Jin, E. J. Mele, S. G. Johnson, and B. Zhen, Floquet Chern insulators of light, *Nat. Commun.* **10**, 4194 (2019).
 - [30] K. Fang and Y. Wang, Anomalous Quantum Hall Effect of Light in Bloch-Wave Modulated Photonic Crystals, *Phys. Rev. Lett.* **122**, 233904 (2019).
 - [31] J. Lu, L. He, Z. Addison, E. J. Mele, and B. Zhen, Floquet Topological Phases in One-Dimensional Nonlinear Photonic Crystals, *Phys. Rev. Lett.* **126**, 113901 (2021).
 - [32] W. Zheng and H. Zhai, Floquet topological states in shaking optical lattices, *Phys. Rev. A* **89**, 061603(R) (2014).
 - [33] N. Goldman, J. C. Budich, and P. Zoller, Topological quantum matter with ultracold gases in optical lattices, *Nat. Phys.* **12**, 639 (2016).
 - [34] G. Jotzu, M. Messer, R. Desbuquois, M. Lebrat, T. Uehlinger, D. Greif, and T. Esslinger, Experimental realization of the topological haldane model with ultracold fermions, *Nature (London)* **515**, 237 (2014).
 - [35] M. S. Rudner and N. H. Lindner, Band structure engineering and non-equilibrium dynamics in floquet topological insulators, *Nat. Rev. Phys.* **2**, 229 (2020).
 - [36] T. Oka and S. Kitamura, Floquet engineering of quantum materials, *Annu. Rev. Condens. Matter Phys.* **10**, 387 (2019).
 - [37] T. Kitagawa, T. Oka, A. Brataas, L. Fu, and E. Demler, Transport properties of nonequilibrium systems under the application of light: Photoinduced quantum hall insulators without landau levels, *Phys. Rev. B* **84**, 235108 (2011).
 - [38] See Supplemental Material at <http://link.aps.org/supplemental/10.1103/PhysRevLett.129.063902> for commutation rules between symmetry operations and the

- time-dependent permittivity, calculation of topological invariants, and more results of physical consequences at the interface.
- [39] J. N. Winn, S. Fan, J. D. Joannopoulos, and E. P. Ippen, Interband transitions in photonic crystals, *Phys. Rev. B* **59**, 1551 (1999).
- [40] T. Christensen, H. C. Po, J. D. Joannopoulos, and M. Soljačić, Location and topology of the fundamental gap in photonic crystals, [arXiv:2106.10267](https://arxiv.org/abs/2106.10267).
- [41] L. Elcoro, B. J. Wieder, Z. Song, Y. Xu, B. Bradlyn, and B. A. Bernevig, Magnetic topological quantum chemistry, *Nat. Commun.* **12**, 5965 (2021).